12th Intern. Symp. on Earth Tides, Aug.4-7, Beijing, China

OMP1 : AN INVERSE MODEL of the GLOBAL OCEAN TIDES

Mazzega P., *UMR39/GRGS* 18 av. E. Belin 31055 Toulouse Cedex France
Francis O., *ORB* 3 av. Circulaire B-1180 Brussels Belgium
Bergé M., *UMR39/GRGS* 18 av. E. Belin 31055 Toulouse Cedex France

One year of GEOSAT satellite altimetry and the harmonic constants from about 650 tide gauge stations are inverted to produce a global atlas (OMP 1) of the 11 leading tidal constituents (namely M2, S2, N2, K2; K1, O1, P1, Q1; Mf, Mm, Ssa) and of the smoothed mean sea surface ellipsoidal heights, on a 0.5°x0.5° grid. Maps of the associated formal errors are computed (5°x5° gridding) as well as a posteriori covariance functions centred on characteristic points of the oceanic areas.

The OMP1 tidal atlas, Schwiderski's atlas (1980 a,b) and the solutions for 5 partial tides computed by Cartwright & Ray (1990) from Geosat data, are then compared with a set of pelagic tidal constants (compiled by Smithson 1992) more or less representative of the global tidal dynamics. The resulting statistics show very similar accuracies for Schwiderski and Cartwright & Ray solutions, and a slightly degraded performance for OMP1. This relative inaccuracy of our solution (9 cm rms for M2, 4 cm rms for K1, etc) is due to the quite heavy error budget of our basic Geosat data set (refered to the GEM-T1 orbit with 85 cm rms radial error) which permits to the a priori tidal covariances to over-smooth the inverse solutions.

1. Introduction

The incentives for trying to improve the models of the global ocean tides have not to be reminded in a meeting devoted to Earth tides. The present day tendency in ocean tide modeling is to bring constraints on hydrodynamical models from pre-processed empirical observations. From a pragmatical point of view, this means that three main algorithms can be developed, quite independently from each others, before producing the final tidal atlas: 1- a numerical model solving the hydrodynamical equations for tides; 2- a numerical scheme for mapping ocean tides from (possibly combined) empirical data sets; 3- a procedure for optimizing the model (1) taking into account the solutions and their associated errors, obtained from the data analysis (2) (eg. Sasaki 1970, Bennett & McIntosh 1982, Zahel 1991).

Corresponding to this structure, the french programme for tidal modeling is based on the following options: 1'- a finite element model solving for the barotropic non-linear shallow water equations in the spectral domain (see Le Provost et al., these Proceedings); 2'- an algorithm inverting combined sets of tide gauge (TG) harmonic constants and satellite altimetry providing maps of several partial tides (eg. this paper); 3'- a variational procedure for assimilating the inverse tidal maps in the finite element model (Jourdin 1992).

The hydrodynamical global model should be completed for the main semi-diurnal and diurnal waves within a few months from now. The assimilation algorithm has

already been developed and tested in real configurations by Jourdin (1992) in the whole Pacific ocean: starting from a rough dynamical tidal solution (using P1 Lagrange polynomials in the finite element meshes), he obtained an improved map of the same accuracy as Schwiderski's model, just by assimilating a few TG data. The feasability to assimilate tidal maps derived from satellite altimetry has also been demonstrated.

This paper presents a first set of global solutions obtained by inverting combined sets of TG and Geosat data. This study was the ultimate step before processing the accurate altimetric data delivered by the Topex/Poseidon satellite from which we have already obtained very promising results on limited oceanic areas, using only 210 days of measurement (Mazzega & Bergé 1993).

2. Data Pre-Processing

2a. Tide Gauge Data

From long enough tide gauge records of the time varying local sea level, the harmonic constants of several tidal waves are extrated. The IHO (1979) data bank stores these tidal constants from several thousands coastal stations. Though the accuracy of these constants may depend on the instrumental device, way of operating them, tidal frequency and duration of the recording period, we have uniformly attributed a $(10\text{cm})^2$ variance to all the TG data. In choosing such a high value, we intend to account for the sea level variability induced by local dynamics (Chelton & Enfield 1986) which is not coherent with the tidal signal of the deep ocean. This choice further helps in improving the conditioning of the Least Squares matrices to be inverted. Its main drawback will be to under-weight the TG constants of the long period tides characterized by centimetric amplitudes.

In the data bank, we have selected only those TG stations with at least 8 (M2, S2, N2, K2; K1, O1, P1, Q1) or 10 (...plus Mf & Mm) partial tides. We so obtained about 650 stations distributed worldwide, among which about 130 also provide the 2 long period waves Mf and Mm. From Figure 1, we see that quite long segments of the coastline may present an extremely sparse data coverage. This situation is particularly unfavourable for example in the Labrador Sea, along the Patagonian Shelf or in the Weddell and Ross Seas, where tidal amplitudes and gradients are unusually strong.

The TG data set was then divided into sets A & B with well balanced geographical distributions. As will appear below in the description of the inversion strategy adopted here, this splitting was motivated for saving computational time.

2b. Geosat Data

One year of GEOSAT satellite altimetry has been used in our inversion (Nov.86 - Nov.87). We shall not give here a detailed account of the tedious altimeter data validation and pre-processing (see eg. Joudin et al. 1991) but just highlight its main steps. We remove from the raw data the GEM-T1 geoid heights (model complete up to degree and order 36; Marsh et al. 1988), the solid Earth tides (as directly predicted from the sun and moon ephemerides) and other geophysical corrections. The reference orbit for our data set is computed from GEM-T1, with an estimated radial accuracy of about 85 cm rms (Haines et al. 1989). In order to reduce our data set and to low down the altimeter white noise, we then performed an averaging of along track consecutive data over 1 degree (equivalent to 15 s). After these corrections and pre-processing, the global rms of our altimetric data set is 165 cm. Though including the residual radial orbit error, the residual geoid heights (commission and omission residues), the residual of geophysical corrections and the various oceanic signals, we find this value to be surprisingly high.

The main source in the altimetric error budget is the radial orbit error. For a given orbit geometry, the typical orbit error spectrum can be well predicted from the theory of

linear orbit perturbations. The main peaks appear at the orbital period (the "natural" period of the satellite motion: about 100 min for Geosat) and harmonics, and at well defined frequencies resulting from the regular sampling of spherical harmonics of the Earth's gravity field. These facts are well known but we still suspected the orbit error spectrum to be nonstationary for orbit arc of several days (orbit integration are performed over 17 days in the GEM-T1 ephemerides). Indeed, considering for example the dominant 1 cy/rev. period, we found its amplitude to change with time from a few decimetres up to 2 meters or so in 17 days. To overcome this problem a method of complex demodulation was developed and successfully applied by Francis & Bergé (1993) to our data set, just removing the 1cy/rev peak. Its was also shown that: 1- only about 2-3 cm of the total ocean tide is projected on this particular peak; 2- that a non-negligible part of the ocean signal appeared in the other spectrum lines mixed together with radial orbit error (Francis 1993). The demodulation of the 1 cy/rev accounts for 69 cm rms of the altimeter data time series, leaving, after correction, a data set with 151 cm rms for inversion.

We then prepared 88 independent sets, each of them including about 6000 altimetric data choosen through a random process providing an homogeneous space coverage of the world ocean, and time coverage of the year of observation. Each altimeter data (AD) set numbered between 1 to 44 is combined with the TG data set A, the AD sets numbered 45 to 88 being combined with TG set B.

3. Inverse Tidal Solutions

The inverse method will not be described in this note. The theoretical background and the various parameters of the set of covariance functions controling the tidal extraction are basically those given in Mazzega & Jourdin (1991). The only noticeable change concerns the a priori covariance function for the radial orbit error. We have propagated the formal errors associated to the spherical harmonic coefficients of the GEM-T1 model. Once the 1 cy/rev. peak is removed from the so obtained formal orbit error spectrum, the dominant lines are a 1 cy/day and its low harmonics. So we built a covariance function from this residual spectrum, just adding a 2-day exponential decay to the correlation (such a damping should appear because of the non-conservative forces acting on the satellite trajectory). In the following, the residual radial orbit error is also considered as an unknown of the inverse problem.

Starting from the general expression for the inverse problem, we have to design a sub-optimal strategy allowing the processing of the huge data set. The characteristic wavelengths of the orbit error being at the scale of the oceanic basins, global inversions were to be performed in order to favour its decorrelation from the tidal and mean sea surface (MSS) signal. So we have performed 88 separate inversions of the elementary data sets previously described, producing 88 atlases to be then properly averaged together. Two remarks are worth making at this stage: 1- each inverted set provides a very low space-time data density in the deep ocean; 2- the adopted strategy is sub-optimal because the AD inverted separately are in fact not statistically independent. Both limitations tend to over-smooth the inverse solutions. This drawback is even emphasized in our case as it is well known (for example in Time series analysis) that the inversion of data with a bad signal to noise ratio leads to solutions with a low resolution.

For a given elementary data set, the maps of the formal errors associated with the real and imaginary parts (rp and ip) of each tidal constituent, have been computed on 5°x5° grids. The error map for the M2-rp is given in Figure 2. A very similar map is obtained for the M2-ip. The typical standard deviation (hereafter s.d.) are 18 cm in the deep ocean far from any TG location, and a few cm at the TGs (note that the coarse resolution of Fig.2 does not allow to see the locations of all the TG used in the

inversions). The 88 inverted sets not being independent from each others, we can not simply apply a $1/\sqrt{88}$ factor to these maps as an estimate of the OMP 1 formal error. We rather pay attention to the general patterns of these error maps for subsequent data analysis or tidal predictions.

The OMP 1 atlas is the final atlas obtained after averaging the 88 elementary solutions. OMP 1 includes the maps for the amplitude and phase of the 11 leading partial tides and the smoothed MSS heights relative to the reference ellipsoid (the MSS surface solution will not be further discussed here), over a global 0.5°x0.5° grid. The inverse solutions for M2 and K1 are given in Figures 3 a-b and 4 a-b respectively. The known general features of the tides are very well restored. The very short wavelength signal observed in shallow water (eg. in the North Sea or South Patagonia) result from the inversion of TG data. The high M2 amplitude in the mouth of the Hudson Bay is due to the 2 isolated TG sations inverted there, which have not been tempered in the Labrador Sea by the too sparse an inaccurate AD. After careful inspection, its also appears that the fictous local maxima observed on the coast of South Africa are induced by an erroneous tidal height unit used in our reading of the IHB data bank. We now let the reader to the subjective appreciation of the global tidal patterns obtained by our inversion algorithm.

4. Accuracy Assessment

Before proceeding to external comparisons, we used our inverse solutions for the residual radial orbit error, the MSS and tides as corrections to our original data set (say solve for the direct problem). In this way, when estimated over the one year of the Geosat mission, the global AD rms was successively reduced from 151 cm to 143 cm, 60 cm and 55.3 cm. It should be noted that the tidal correction (last step) has iyself a 24.5 cm rms (with a 0.4 cm global mean under the satellite tracks) which is lower than the variance a priori attributed to the total ocean tide (27 cm). We interpret this difference (the difference of the variances gives 11 cm rms of residual tide) as a first evidence of the over-smoothing of our inverse solutions.

We then prepared an extrenal set of pelagic tidal constants for comparison with the OMP1 atlas, Schwiderski's model (1980 a-b) and five waves of the Cartwright & Ray (1990) solution. These data were taken from the new IAPSO compilation prepared by Smithson (1992). The harmonic constants obtained from pelagic records shorter than 27 days were first rejected. We then averaged, for each partial tide, the constants available in the same 0.5°x0.5° predefined mesh. A 4-point linear interpolation scheme was used to interpolate each model at the averaged pelagic data location. An histogram of the residues for the M2 tide (both real and imaginary residues are set together) is plotted in Figure 5. We immediately see the larger scattering of the OMP 1 residues.

To get a global estimate of the accuracy of the three models, we have computed the mean and r.m.s of these residues after rejection of the wings of the histogram with M2 absolute residues $\geq$ 25 cm. The results are plotted for the 8 leading partial tides in Figure 6 (except for K2, Q1 and P1 from Cartwright & Ray). We see from these comparisons that the rms of the OMP 1 residues are significantely larger than those of the other solutions, with still very similar results obtained for the minor waves. The mean discrepancies (cf the black symbols in Fig.6) of the 3 models are of the same order of magnitude, say up to 0.5 - 1 cm. As the rejection of some data of the raw histograms may appear debatable, we made the same kind of comparison with a set of pelagic and island TG data prepared by Cartwright & Ray (1990). This more restricted set is clearly not independent from ours and probably gives more weight to the deep ocean (see Fig.1). Nevertheless, we obtained the same statistics as those given in Fig.6.

We finally tried to improve our solutions by performing a second iteration of the data inversion. The inverse solution was removed from the original data (orbit error,

MSS, tides). Some typical a posteriori tidal covariance tensors were estimated locally and parametrized. These nonstationary tensors (with very short correlation lengths near the TGs for example) are then used as a priori information in the inversion of the data residues. Moreover, the inversion strategy could be oriented to the analysis of regional data set (the bulk of the radial orbit error being now hopefully removed from AD). It appeared first that the residual tidal signal to noise ratio was too low for further information to be extracted from Geosat altimetry. Second, the sole inversion of residual TG data led to minor or very local improvement of our inverse solutions.

5. Conclusion

When comparing the amplitudes of the external TG data with the amplitudes given by the OMP 1 atlas, we found systematic lower values for OMP 1. This fact is the clearer evidence that the inversion algorithm has over-smoothed the tidal signal. As explained above, this in turn results from the too heavy AD error budget which prevents from recovering the less energetic short wavelengths of the tides.

This study should be considered a further step toward global inversions of the high accuracy altimetric data of the Topex/Poseidon mission. Preliminary inversions of these new data (see Mazzega & Bergé 1993) have shown that ("*happily*" -sic F.O.) all the machinery developed in order to reduce the effects of the radial orbit error on the inverse solutions (Francis & Bergé 1993) could now be simply by-passed. The strategy based on separate inversions of global data sets can be abandonned for the much more efficient one where a regional, high space-time density data sets is inverted for each (running) computation point.

More care will be also taken in extracting the harmonic constants from the IHB data bank. We also plan to use in our inversion the TG stations with less that 8 defined partial tides, so obtaining a much better coverage of some quite remote seas or shelves where the tidal dynamics may be complex, or the AD coverage marginal (eg. in the ice covered areas).

Acknowledgements: Most computations have been performed on the CRAY2 of the Centre de Calcul Vectoriel pour la Recherche (CCVR, Palaiseau, France). JC. Marty (from CNES-BGI) has provided us with the GEM-T1 geoid map. N. Vales (CNES-BGI) performed for us the formal prediction of the Geosat radial orbit error starting from the GEM-T1 a posteriori covariance matrix. We are grateful to them.

References

* **Bennett, A.F. & P.C. Mc Intosh**, 1982, "Open ocean modeling as an inverse problem: tidal theory", J. Phys. Oceanogr., 12, 1004 - 1018.
* **Cartwright, D.E. & R.D. Ray,** 1990, "Oceanic tides from Geosat altimetry", J. Gephys. Res., 95 C3, 3069 - 3090.
* **Chelton, D.B. & D.B. Enfield**, 1986, "Ocean signals in tide gauge records", J. Geophys. Res., 91 B9, 9081-9098.
* **Francis, O.**, 1993, "Modèle global des marées océaniques obtenu par inversion de mesures marégraphiques, gravimétriques et altimétriques", Thèse Univ. Catholique Louvain, Sept.93, 196pp.
* **Francis, O. & M. Bergé**, 1993, "Estimate of the radial orbit error by complex demodulation", J. Geophys. Res., 98 B9, 16083-16094.

* **Haines, B.J., Born, G.H., Marsh, J.G. & R.G. Williamson,** 1989, "A summary of precise orbit computation for the Geosat exact repeat mission", John Hopkins APL Techn. Digest, 10(4), 393-404.
* **International Hydrographic Office,** 1979, "Tidal constituents bank; station catalog", Ocean & Aquat. Sci., Dept. Fish. & Oceans, Ottawa.
* **Jourdin, F.,** 1992, "Assimilation de mesures marégraphiques et altimétriques dans un modèle hydrodynamique de marées océaniques", Thèse Univ. Sci. Toulouse, 241 pp.
* **Jourdin, F., Francis, O., Vincent, P. & P. Mazzega,** 1991, "Some results of heterogeneous data inversions for oceanic tides", J. Geophys. Res., 96 B12, 20267-20288.
* **Marsh, J.G. & al.,** 1988, "A new gravitational model for the Earth from satellite tracking data: GEM-T1", J. Geophys. Res., 93 B6, 6169-6215.
* **Mazzega, P. & F. Jourdin,** 1991, "Inverting Seasat altimetry for tides in the NE Atlantic: preliminary results", in Tidal Hydrodynamics, B. Parker ed., J. Wiley & Sons, New York, 569-592.
* **Mazzega, P. & M. Bergé,** 1993, "Ocean tides in the asian semi-enclosed seas from Topex/ Poseidon", subm. to J. Geophys. Res.-Oceans, (Nov. 93).
* **Sasaki, Y.,** 1970, "Some basic formalisms in numerical variational analysis", Monthly Weath. Rev., 98(12), 875-883.
* **Schwiderski, E.W.,** 1980a, "Ocean tides, part I: global ocean tidal equations", Mar. Geodesy, 3, 161-217.
* **Schwiderski, E.W.,** 1980b, "Ocean tides, part II: a hydrodynamical interpolation model", Mar. Geodesy, 3, 219-255.
* **Smithson, M.J.,** 1992, "Pelagic tidal constants - 3", IAPSO Publ. Sci. n°35, 191 pp.
* **Zahel, W.,** 1991, "Modeling tides with and without assimilating data", J. Geophys. Res., 96 B12, 20379-20391.

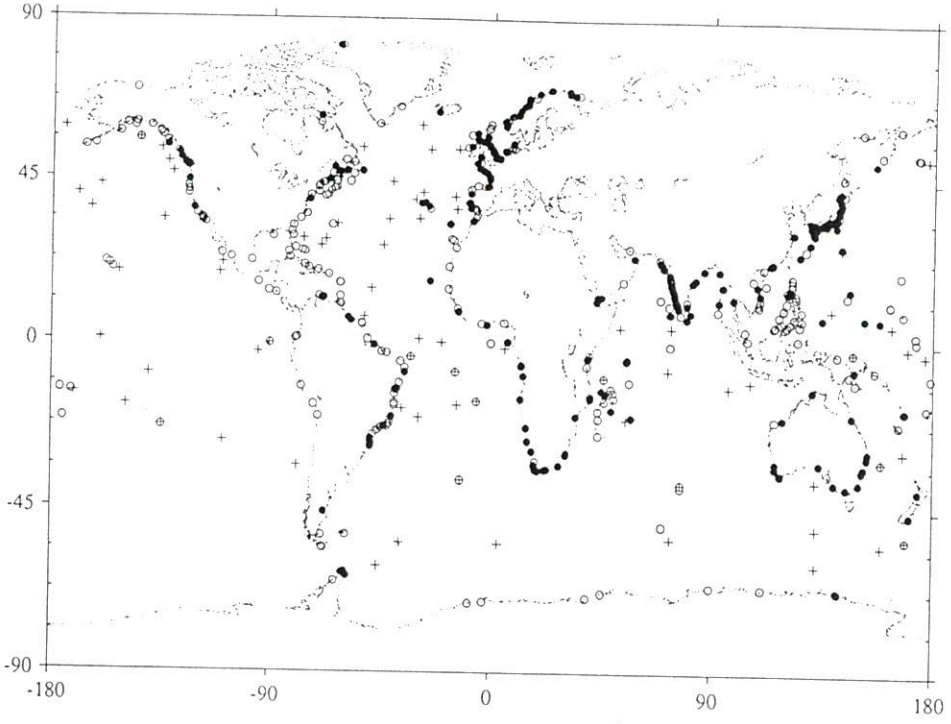

FIGURE 1: DISTRIBUTION of the TIDE GAUGES USED IN THEO OMP1 ATLAS
à 0: TG with 8 waves; ●: TG with 10 waves; +: TG for comparison

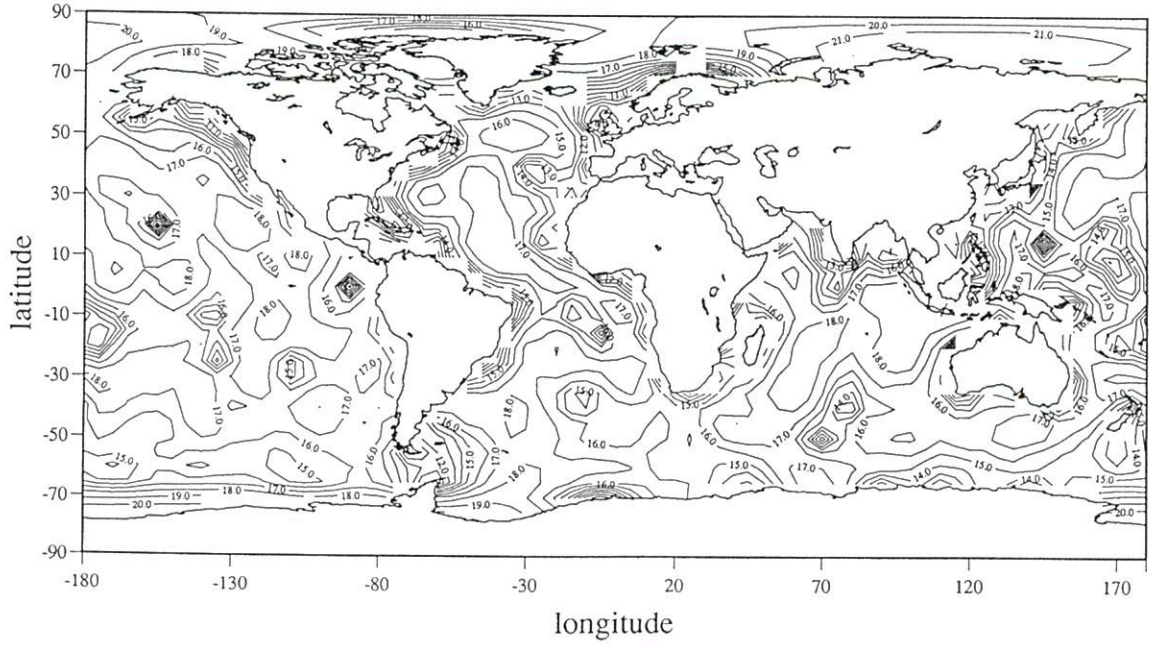

FIGURE 2: FORMAL ERROR MAP of the M2-Real Part INVERSE SOLUTION

FIGURE 3a : Amplitude M2 (cm) : OMP1

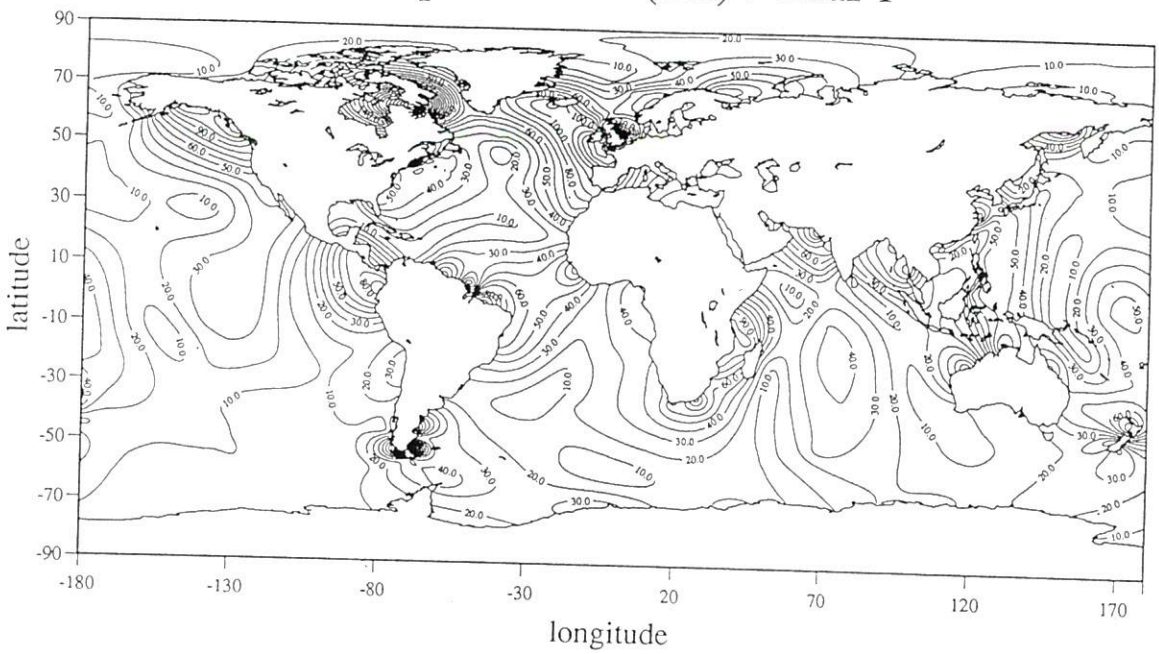

FIGURE 3b : Phase M2 (dg) : OMP1

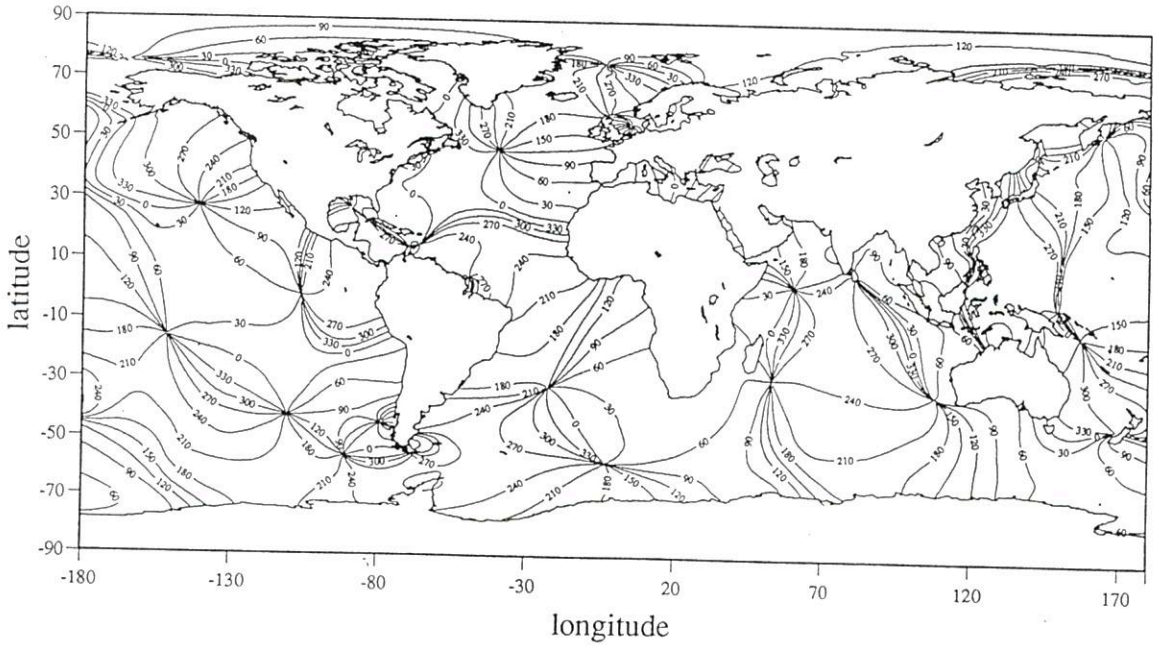

FIGURE 4a : Amplitude K1 (cm) : OMP1

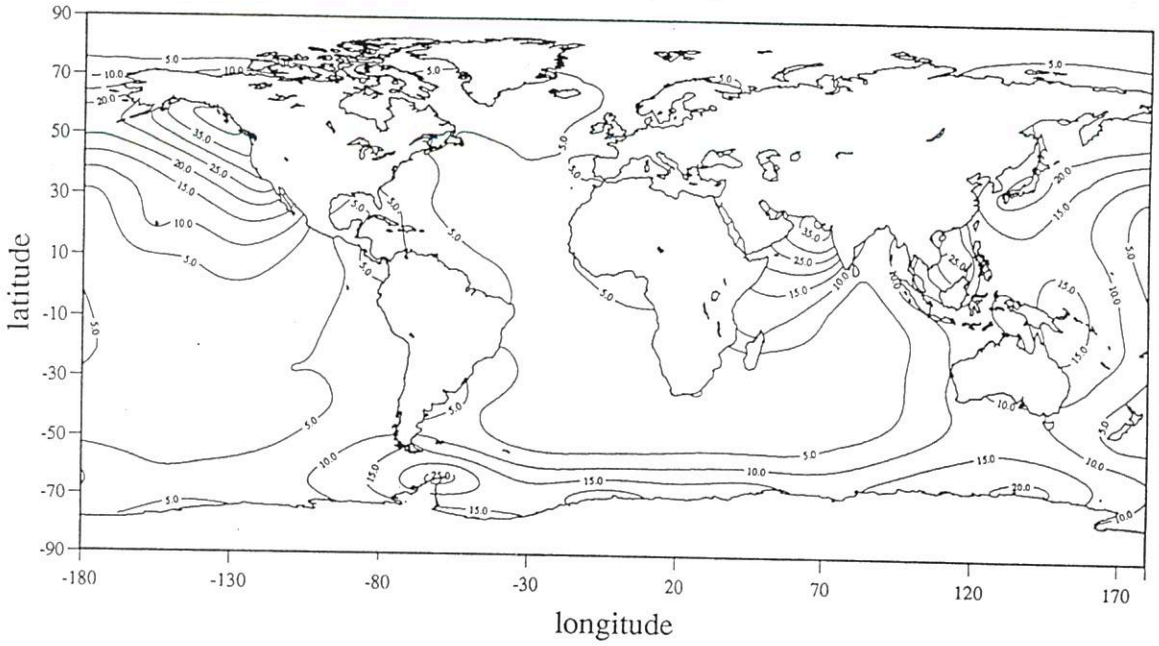

FIGURE 4b : Phase K1 (dg) : OMP1

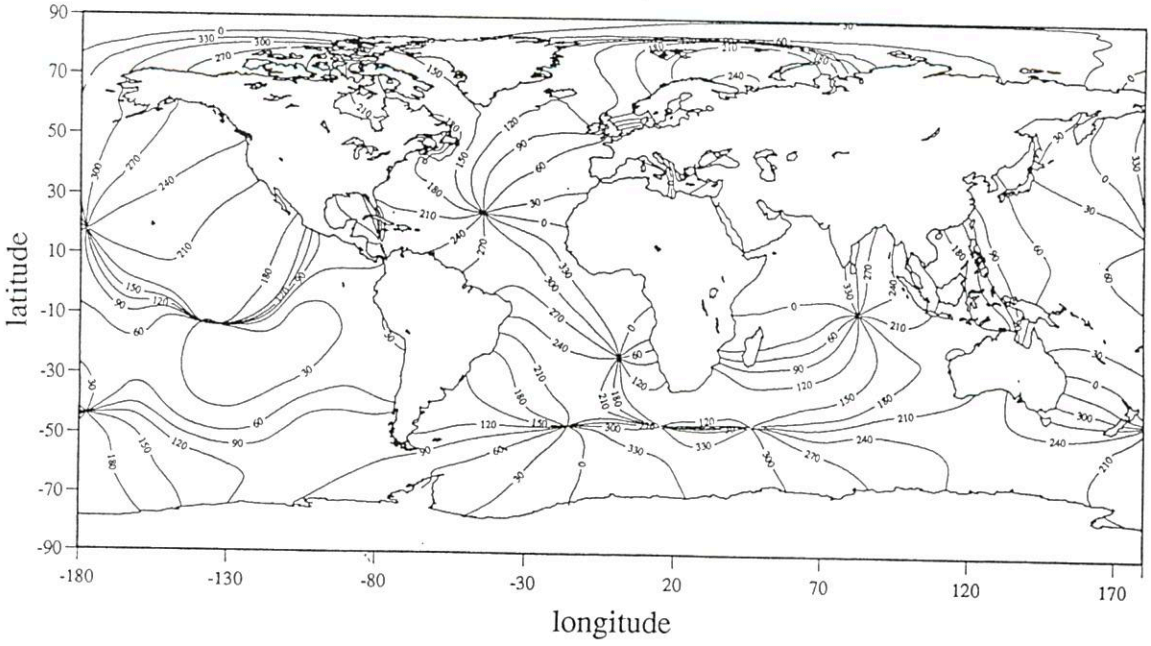

FIGURE 5 : M2 : Histogram of the Models Residues (/IAPSO)

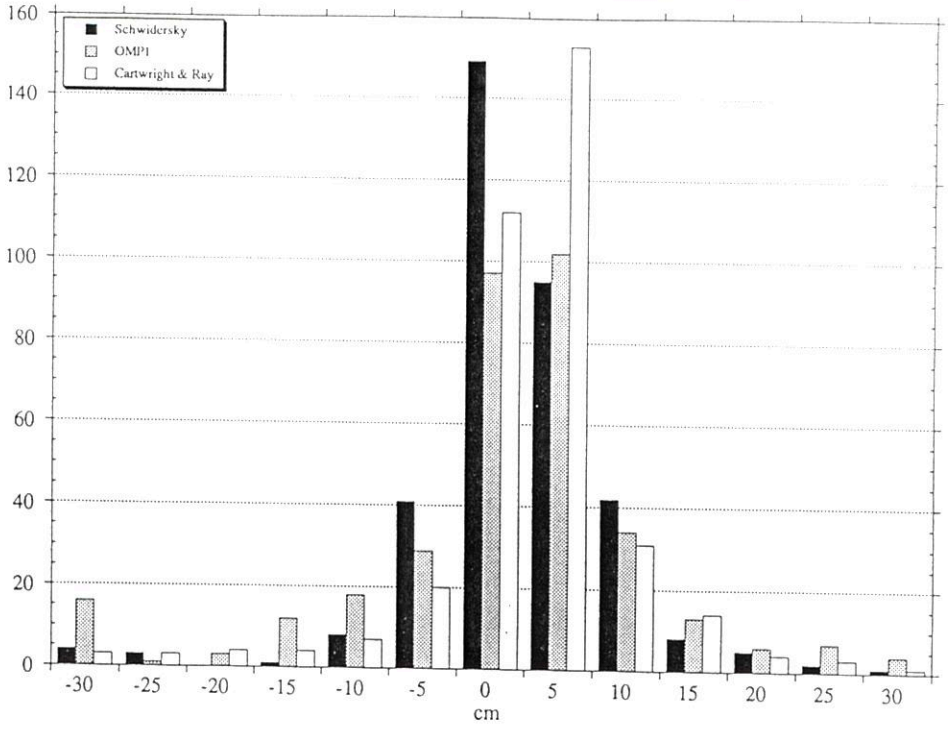

FIGURE 6: Global statistics : Comparisons with in-situ Data (IAPSO)